Signature of non-Newtonian orbits in ray-splitting cavities

Sz. Bauch,[1] A. Błędowski,[1] L. Sirko,[1,2] P. M. Koch,[2] and R. Blümel[3]
[1]*Institute of Physics, Polish Academy of Sciences, Aleja Lotników 32/46, 02-668 Warszawa, Poland*
[2]*Department of Physics and Astronomy, State University of New York at Stony Brook, Stony Brook, New York 11794-3800*
[3]*Fakultät für Physik, Universität Freiburg, Hermann-Herder Strasse 3, D-79104 Freiburg, Germany*
(Received 15 July 1997)

Ray splitting is a universal phenomenon that occurs in all wave systems with sharp interfaces. A key consequence of ray splitting is the occurrence of non-Newtonian periodic orbits whose presence can be revealed in the oscillating part of the density of states. We use thin dielectric- and metal-loaded microwave cavities to identify experimentally the signature of non-Newtonian periodic orbits caused by ray splitting at sharp interfaces and corroborate all our experimental results with detailed numerical computations and semiclassical theory. For two-dimensional ray-splitting problems the electromagnetic Helmholtz and quantal Schrödinger equations are equivalent. Thus our results are directly relevant to quantum chaos studies. [S1063-651X(97)11612-9]

PACS number(s): 05.45.+b

I. INTRODUCTION

The behavior of waves at the interface between two media is of fundamental importance in many fields of physics. The most widely studied phenomena in this context are reflection, refraction, and diffraction. In the limit of small wavelengths, the geometric optics limit, it is possible to assign rays to wave fronts. Reflection and transmission at sharply defined interfaces then give rise to the phenomenon of ray splitting. Ray splitting is universal. It occurs, e.g., in optics when a light ray encounters the interface between two different transparent media of different index of refraction; it occurs in hydrodynamics when a surface wave passes between two regions of different depths; it occurs in geophysics where waves generated by an earthquake experience ray splitting at fault lines. While these manifestations of ray splitting are well known and studied in detail since the times of Snell and Descartes, the wave implications of ray splitting were only recently investigated. Couchman *et al.* [1] studied ray splitting in the context of acoustics and quantum chaos. Prange *et al.* [2] computed analytically the ray-splitting (RS) correction to the Weyl formula [3] and suggested specific experiments for the purpose of studying RS phenomena. Blümel *et al.* [4,5] investigated RS phenomena theoretically in a chaotic, circular, step billiard. They identified the signatures of non-Newtonian RS orbits in the Fourier transform of the scaled level density, thereby demonstrating numerically the importance of periodic non-Newtonian RS orbits. Sirko *et al.* [6] verified experimentally the predicted manifestations of ray splitting of electromagnetic waves. Non-Newtonian orbits also appear in the context of diffraction [7], a topic closely related to RS phenomena.

Central points of this paper are to check the theoretical predictions [1,2,4,5] and to elaborate on the experimental results [6] on the wave implications of ray splitting. To this end we use thin microwave cavities partially loaded with dielectric or metal in order to generate ray splitting of electromagnetic waves at sharp interfaces. Thus our paper continues the use of microwave resonance spectroscopy to verify wave effects predicted on the basis of semiclassical quantum physics. This was pioneered by Stöckmann and Stein [8], who began the use of microwave cavity resonators for investigating the validity of the conjecture of a universal connection between classical chaos and quantal energy level statistics in two-dimensional billiards. Using microwave cavities for which analytical solutions are not possible, the paper by Sridhar and Kudrolli [9] presented an experimental demonstration of the consequences of the theorem of isospectral domains. Information came both from the eigenfrequency spectrum, as in [8], and from experimental maps of the eigenfunctions obtained with a frequency pertubation method [10] used for these purposes in [11]. The predicted influence of time-reversal symmetry breaking on energy-level statistics was checked by So *et al.* [12] and Stoffregen *et al.* [13]. The paper by Sirko *et al.* [6] presented an experimental demonstration of the predicted existence of non-Newtonian orbits by analyzing resonance spectra of a microwave cavity partially filled with a dielectric, Teflon. The purpose of the present paper is to amplify the results obtained in [6] and to present the results of measurements and theory on the wave implications of ray splitting in metal-loaded microwave cavities. Because the electromagnetic Helmholtz and quantal Schrödinger equations are equivalent in two dimensions, our results are directly relevant to quantum chaos studies [2,3].

The paper is organized in the following way. Section II presents some theoretical background relevant for RS systems, including the precise nature of the predictions of quantum theory on the importance of non-Newtonian orbits for RS systems. These predictions are illustrated with the help of simple, one-dimensional RS models. Section III presents our experiments and theory on the spectra of empty cavities. These results establish the reliability of our experimental and theoretical methods. Section IV presents our experimental evidence for the existence of non-Newtonian orbits in the context of thin microwave cavities partially filled with Teflon. Section V investigates thin cavities partially filled with metal. This system also shows the signatures of non-Newtonian orbits. Section VI analyzes our theoretical and experimental results in the light of semiclassical theory. Sec-

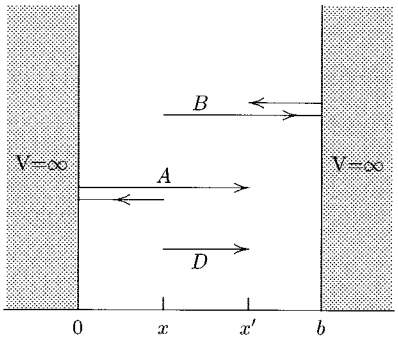

FIG. 1. Quantum propagation in the one-dimensional square-well potential. Starting from x, the point x' in the well can be reached in a variety of different ways. The shortest paths are sketched and denoted by D (direct path), A (shortest path connecting x with x' via a single bounce off the left-hand wall of the well), and B (shortest path connecting x with x' via a single bounce off the right-hand wall of the well). All connecting paths in the square well are Newtonian.

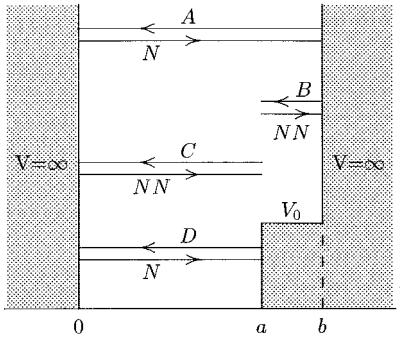

FIG. 2. Newtonian (N) and non-Newtonian (NN) periodic orbits in a one-dimensional square well potential with a potential step of finite height V_0.

tion VII discusses our results. Section VIII summarizes our findings and concludes the paper.

II. THEORETICAL CONTEXT

To appreciate the issues involved when dealing with the semiclassics of RS systems, we shall use some one-dimensional systems to illustrate all the pertinent ideas and nomenclature needed to discuss two-dimensional RS systems in Secs. III–VII. Consider the one-dimensional square-well potential sketched in Fig. 1. The normalized eigenstates of a particle of mass m in the well are $\psi_n(x) = \sqrt{2/b}\,\sin(n\pi x/b)$, $n=1,2,\ldots$. Using these states we construct the energy-dependent Green's function for propagation at energy E from x to x' (see Fig. 1)

$$G(x,x';E)=\sum_{n=1}^{\infty}\frac{\psi_n(x)\psi_n(x')}{E-E_n+i\epsilon}. \tag{2.1}$$

With the help of Poisson's formula Eq. (2.1) can be cast into

$$G(x,x';E)=\frac{m}{i\hbar^2 k}\sum_{\nu=-\infty}^{\infty}\{\exp(i|x-x'+2\nu b|k) - \exp(i|x+x'+2\nu b|k)\}, \tag{2.2}$$

where $k=\sqrt{2mE/\hbar^2}$. The result (2.2) can be interpreted in terms of multiple paths. The first term in Eq. (2.2) for $\nu=0$ represents the direct path from x to x', denoted by D in Fig. 1. The term in the exponent is the classical action of this path in units of $\hbar$. The second term in Eq. (2.2) for $\nu=0$ represents an indirect path from x to x', which proceeds via one reflection from the left-hand wall of the square well. It is denoted by A in Fig. 1. Another possibility of reaching x' starting from x is to ''overshoot,'' i.e., reflect at the right-hand wall of the square well and return to x'. This path, denoted by B in Fig. 1, is represented by the second term in Eq. (2.2) for $\nu=-1$. The minus sign in front of the second term in Eq. (2.2) follows from both A and B involving a single reflection at one of the walls of the square well. Of course x' is reachable from x by any number of overshoots followed by bounces off the walls of the square well. This explains the infinite sum in Eq. (2.2). The level density $\rho(E)$ of the square well is easily computed using the trace formula $\rho=-\mathrm{Im\,Tr}\,G/\pi$. We obtain

$$\rho(E)=\frac{mb}{\hbar^2 k\pi}\left[1+2\sum_{n=1}^{\infty}\cos(2nbk)\right]. \tag{2.3}$$

The level density (2.3) can be written in the form of a Gutzwiller formula [3]

$$\rho(E)=\overline{\rho}(E)+\widetilde{\rho}(E), \tag{2.4}$$

where $\overline{\rho}(E)=dn/dE=mb/\hbar^2 k\pi$ is the average part of the level density and

$$\widetilde{\rho}(E)=\frac{1}{\hbar\pi}\sum_{n=1}^{\infty}T(E)\cos[nS(E)/\hbar] \tag{2.5}$$

is the oscillating part. For the square well there is only one primitive periodic orbit at energy E. Its action, $S(E)$ in Eq. (2.5), is given by $\oint p\,dx=\hbar(2bk)$. The round-trip time $T(E)$ on this orbit is given by $T(E)=\partial S(E)/\partial E=2bm/\hbar k$. Inserting these results into Eq. (2.5) reproduces Eq. (2.3).

The form of the level density (2.3) suggests a straightforward method for extracting from it the actions of primitive periodic orbits and their repetitions: Fourier transformation according to

$$\mathcal{F}(l)=\int\begin{Bmatrix}\rho(E)\\ \widetilde{\rho}(E)\end{Bmatrix}\exp(-ikl)dE. \tag{2.6}$$

Using $\rho(E)$ in Eq. (2.6) produces a sharp peak at $l=0$ that corresponds to the zero-length periodic orbit responsible for $\overline{\rho}(E)$. Using $\widetilde{\rho}(E)$ in Eq. (2.6) we obtain peaks only at the actions of nontrivial periodic orbits. In the case of the square well the Fourier transform (2.6) is strongly peaked at multiples of the ''reduced action'' $l_0=S(E)/\hbar k=2b$, the length of the primitive periodic orbit.

Let us now introduce a potential step into the square well of Fig. 1. We obtain the one-dimensional step billiard shown in Fig. 2. The energy levels are obtained from the solutions E_n of the transcendental equation

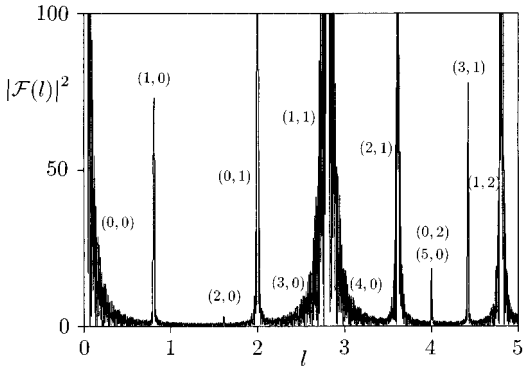

FIG. 3. Absolute square of the Fourier transform of the scaled level density of the step potential sketched in Fig. 2 for $a=1$, $b=\pi/2$, and $\eta=1/2$. The peaks can be associated with linear combinations of multiples of the actions l_B and l_C according to $l_{ij}=il_B+jl_C$, $i,j=0,1,\ldots$, where B and C refer to the two primitive non-Newtonian orbits B and C of Fig. 2. The assignments (i,j) of the peaks are indicated in the figure.

$$\sqrt{1-\eta}\,\tan(ka)+\tan[k\sqrt{1-\eta}(b-a)]=0, \tag{2.7}$$

where

$$\eta=V_0/E. \tag{2.8}$$

The level density is given by

$$\rho(E)=\sum_{n=1}^{\infty}\delta(E-E_n). \tag{2.9}$$

With the potential step present Fourier transformation of $\tilde{\rho}$ will no longer yield sharp peaks at the actions of the primitive periodic orbits since the classical action $S(E)=\oint p\,dx$ no longer scales in k. This, however, can be trivially ''cured'' by calculating ''scaled'' energy levels [4]. This is done by computing the roots of Eq. (2.7) keeping η constant. This condition is automatically fulfilled for microwave cavities partially filled with dielectric [2].

For the step potential shown in Fig. 2 we computed 200 scaled energy levels using $a=1$, $b=\pi/2$, and $\eta=1/2$. We Fourier transformed the level density (2.9) according to Eq. (2.6). The absolute square of the resulting transform $|\mathcal{F}(l)|^2$ is shown in Fig. 3. Since $\eta<1$, meaning $E>V_0$, the only primitive Newtonian periodic orbit is the one bouncing between the left- and right-hand walls of the well. It is denoted by A in Fig. 2. Its action is given by

$$S=\hbar k l_0, \tag{2.10}$$

where

$$l_0=2[a+\sqrt{1-\eta}(b-a)]. \tag{2.11}$$

Simple Bohr-Sommerfeld quantization of this orbit yields approximate solutions of Eq. (2.7) given by

$$k_n=2\pi n/l_0. \tag{2.12}$$

Using the wave numbers (2.12) to compute the level density (2.9), the Fourier transform (2.6) can be performed analytically, giving

$$\mathcal{F}(l)\sim\sum_{m=0}^{\infty}\delta(l-ml_0). \tag{2.13}$$

Thus we expect sharp peaks in the Fourier transform at multiples of $l_0\approx 2.8$ for our choice of parameters. Figure 3, however, shows that $\mathcal{F}(l)$ contains many more peaks in addition to those expected according to Eq. (2.13). They occur at the locations

$$l_{ij}=il_B+jl_C, \quad i,j=0,1,2,\ldots, \tag{2.14}$$

where $l_B=2\sqrt{1-\eta}(b-a)$ is the reduced action of the orbit B in Fig. 2 and $l_C=2a$ is the reduced action of the orbit C in Fig. 2. Since $E>V_0$, neither one of the orbits B or C is Newtonian: They are manifestly non-Newtonian. While the orbit B is never Newtonian at any energy, note that the orbit C evolves into the Newtonian orbit D for $E<V_0$. This simple one-dimensional example also shows that not all conceivable non-Newtonian orbits (a multiply overcountable set of orbits in the sense of Feynman's path integrals) are equally important. Important are only those non-Newtonian orbits, or rays, that originate by the process of *ray splitting* at sharp potential steps.

This discussion for the one-dimensional step potential shows that non-Newtonian orbits are important for the fluctuation properties of the level density of RS systems. To the extent that they cannot be neglected in a proper semiclassical treatment of RS systems, quantum mechanics must certainly ''know'' about the non-Newtonian orbits. This observation motivated the authors of Ref. [1] to extend Gutzwiller's trace formula [3] (which includes only summation over periodic *Newtonian* orbits) to a formula that also includes summation over all periodic *non-Newtonian* RS orbits. Their modified Gutzwiller formula is [1,4]

$$\tilde{\rho}(E)=\mathrm{Im}\sum_n\frac{A_n^{1/2}T_n}{2i\hbar\sinh(\lambda_n/2)}\exp\left[i\left(\frac{S_n(E)}{\hbar}+\phi_n\right)\right]. \tag{2.15}$$

In this formula $\tilde{\rho}$ is the oscillating part of the level density, the sum extends over all periodic orbits of the system (Newtonian and non-Newtonian) including repetitions, T_n are the traversal times of the primitive periodic orbits, λ_n are the associated stability indices, $S_n(E)$ are the classical actions at energy E, ϕ_n are phases, and

$$A_n=\left[\prod_{i=1}^{\varrho_n}|r_i|^2\right]\left[\prod_{j=1}^{\tau_n}(1-|r_j|^2)\right] \tag{2.16}$$

are orbit weights, where ϱ_n counts the number of reflections, τ_n counts the number of transmissions of orbit number n, and $|r_i|^2$ is the reflection probability at encounter number i at a RS interface.

Inasmuch as Eq. (2.15) is a good approximation to the level density $\tilde{\rho}$ of a given RS system, the structure of Eq. (2.15) again suggests using the Fourier transform (2.6) to extract periodic orbit information from $\tilde{\rho}$. Thus a Fourier transformation of the experimental level density directly reveals the content of Newtonian and non-Newtonian periodic orbits. This was the guiding principle we used in Ref. [6] to

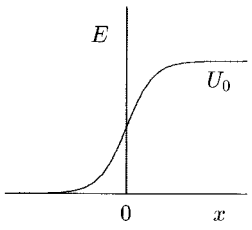

FIG. 4. Sketch of an analytically solvable step potential of width w and potential height U_0 [15]. It serves to illustrate the difference between the Newtonian and the non-Newtonian (RS) semiclassical limits.

demonstrate experimentally the signature of non-Newtonian orbits in a thin microwave cavity loaded with a bar of Teflon.

An alternative semiclassical approach is Bogomolny's method of quantum surfaces of section. It works very well for families of periodic orbits, and just like Gutzwiller's formula it can be modified to include non-Newtonian orbits. According to Bogomolny's approach, the oscillating part of the level density is given by [4]

$$\tilde{\rho}(E)=\frac{1}{\pi}\mathrm{Im}\sum_{s=1}^{\infty}\frac{1}{s}\frac{d}{dE}\mathrm{Tr}\,\hat{\mathcal{T}}(E)^s, \tag{2.17}$$

where $\hat{\mathcal{T}}(E)$ is Bogomolny's transfer operator that is based on semiclassical transition amplitudes [14]. In position representation it is given by

$$\mathcal{T}(q,q';E)=\frac{\mathcal{A}(q,q';E)}{\sqrt{2\pi i\hbar}}\left|\frac{\partial^2 S(q,q';E)}{\partial q\,\partial q'}\right|^{1/2} \times\exp\left[\frac{i}{\hbar}S(q,q';E)+\text{phases}\right], \tag{2.18}$$

where $\mathcal{A}$ is an amplitude that keeps track of successive reflections and transmissions encountered by an orbit that travels from starting point q to end point q' on the quantum surface of section. We shall use Bogomolny's approach in Sec. VI for the computation of the contribution of non-Newtonian orbits to the level density.

A last question remains. When is ray-splitting important? As an aid to answering this question we consider reflection and transmission in an analytically solvable step potential with variable width [15]. A particle P of mass m and energy $E>U_0$ incident from the left scatters off the potential $U(x)=U_0/[1+\exp(-x/w)]$ sketched in Fig. 4. U_0 is the strength of the potential and w is its width. Asymptotically the wave function is given by $\psi(x)=\exp(ikx)+r\exp(-ikx)$ for $x\to-\infty$ and $\psi(x)=t\exp(i\kappa x)$ for $x\to\infty$, where $k=[2mE]^{1/2}/\hbar$, $\kappa=[2m(E-U_0)]^{1/2}/\hbar$, and t is the transmission amplitude. The reflection coefficient r, computed explicitly in Ref. [15], is

$$r=\frac{\sinh[\pi w(k-\kappa)]}{\sinh[\pi w(k+\kappa)]}. \tag{2.19}$$

We are interested in the semiclassical limit that involves the scattering of waves for $\hbar\to0$ in the limit of a sharp potential step, i.e., $w\to0$. The resulting double limit $\hbar\to0,w\to0$ is undefined without further specification. There are two cases of interest. (i) For fixed w we let $\hbar\to0$ and only then let $w\to0$. This is the ''Newtonian limit.'' In this limit the ray dynamics of P is ordinary Newtonian mechanics; for $E>U_0$ ($E<U_0$), P is transmitted (reflected) with unit probability to the right (left). (ii) For fixed $\hbar$ we let $w\to0$ and only then let $\hbar\to0$. This is the RS limit. In this case the ray dynamics of P is a non-Newtonian, nondeterministic mechanics that involves ray splitting at the potential step [1]. The RS limit of Eq. (2.19) is

$$r=(k-\kappa)/(k+\kappa), \tag{2.20}$$

which, it should be noted, is independent of $\hbar$. Consequently, even for $E>U_0$ and $\hbar\to0$, P is not transmitted with unit probability; it is reflected with finite probability to the left. While for a Newtonian orbit reflection and transmission are decided on the basis of energy and momentum considerations only, reflection and transmission in the RS limit are stochastic processes. By ''stochastic'' we mean the following. A ray impinging on the RS boundary has to ''decide'' whether it is transmitted through the RS boundary or is specularly reflected. Reflection and transmission are governed by the reflection probabilities $|r_i|^2$. Thus the proper ray dynamics in the RS limit is not deterministic; it is truly *nondeterministic*. This is the reason why we chose the word *stochastic* for characterizing the ray dynamics in the RS limit. The consequences of the stochasticity of the ray dynamics were already explored in several theoretical publications [1,4,16].

Returning to the extended Gutzwiller formula (2.15), we see that non-Newtonian orbits contribute with appreciable weight only if the reflection coefficients r are large. The weights (2.16) of short non-Newtonian RS orbits in Eq. (2.15) are essentially proportional to the product of the $|r_i|^2$. Therefore, for a particular non-Newtonian orbit to be important, the product of the reflection probabilities should not be too small. This translates physically into the requirement that the width of the RS interface has to be very small compared to the local wavelength. At $E=2U_0$, e.g., the reflection probability $|r|^2$ computed from Eq. (2.19) reaches the 1% level only if the width of the potential w is smaller than about 1/20 of a wavelength. This answers our question. Ray splitting is important whenever the potential varies on a scale that is much smaller than a wavelength. This requirement is easily fulfilled in the microwave context where typical wavelengths are in the centimeter regime and the widths of dielectric interfaces can be machined to micrometer precision.

In the following we are mainly concerned with two-dimensional RS billiards. A RS billiard is characterized by the existence of a RS boundary in its interior as shown in Fig. 5. The (sharp) RS boundary of length R divides the billiard into two isolated areas A and A' wherein the potential is $V=0$ and $V=V_0$, respectively. The outer perimeters of the two separate domains are denoted by L and L', respectively, as shown in Fig. 5. The basic characteristic of RS billiards is the mean level density, computed from the mean staircase function [3] $\overline{\mathcal{N}}(E)$ according to

$$\overline{\rho}(E)=d\overline{\mathcal{N}}(E)/dE. \tag{2.21}$$

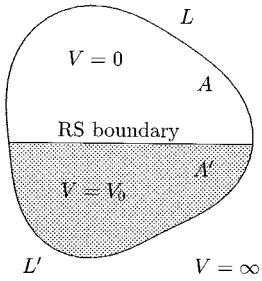

FIG. 5. Typical ray-splitting billiard. The ray-splitting boundary divides the billiard into two separate regions of area A, perimeter L, $V=0$ and area A', perimeter L', $V=V_0$, respectively.

For Dirichlet boundary conditions the mean staircase is given by ($\hbar=1$, $m=\frac{1}{2}$)

$$\overline{\mathcal{N}}(E,V_0)=\frac{1}{4\pi}[AE+A'(E-V_0)\theta(E-V_0)] - \frac{1}{4\pi}[L\sqrt{E}+L'\sqrt{E-V_0}\theta(E-V_0)] + R\sqrt{V_0}\,\overline{\nu}_{RS}(E/V_0)+\Delta\overline{\mathcal{N}}(E,V_0), \quad (2.22)$$

where θ is Heaviside's step function and $\overline{\nu}_{RS}$ is the RS correction derived in [2]. The RS correction in Eq. (2.22) was checked in [2] for an integrable RS billiard with mixed boundary conditions and was found to be accurate. It was checked in [17] for a chaotic, triangular RS billiard and was again found to be accurate. Additional corrections to the mean level density $\overline{\rho}(E)$ that arise from topological characteristics of the billiard, such as corners and holes, are subsumed into the term $\Delta\overline{\mathcal{N}}(E,V_0)$ in Eq. (2.22).

III. EMPTY CAVITIES

This section sets the stage for our experiments on dielectric- and metal-loaded cavities reported in Secs. IV and V, respectively. The main purpose is to present our experimental technique and to make contact with existing theory and experiments on empty cavities. Thus our results on empty cavities are the point of departure and will serve as the reference gauge for our experiments and theory with loaded cavities.

It is well known [18] that in the case of thin cavities the Maxwell equations for the vector electromagnetic waves reduce to the two-dimensional situation of a Helmholtz equation for a scalar wave problem, i.e., a Schrödinger equation. (An empty cavity is ''thin'' for frequencies ν less than the cutoff frequency $\nu_c=c/2H$, where c is the speed of light and H is the cavity height.) Hence microwave cavities are excellent models for quantum chaos [8,12,13,19]. Figure 6(a) shows the shape and the dimensions of our cavity, a Bunimovich stadium [3]. A denotes its area and L its perimeter. We used a transmission method [20] to measure the resonant frequencies of the empty cavity. We were careful to compare spectra obtained with different placements and insertion

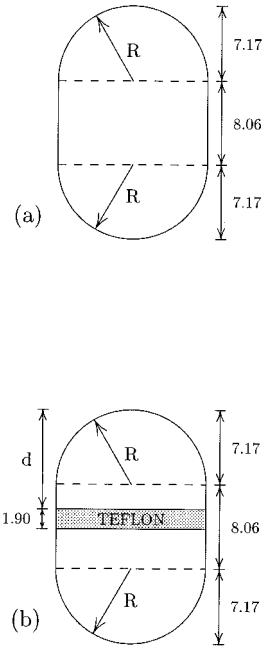

FIG. 6. Sketch of the Bunimovich stadium microwave cavity. Dimensions are given in cm. (a) The empty cavity. (b) The dielectric-loaded cavity. In order to study the shift in position of periodic non-Newtonian RS orbits, the position d of the Teflon dielectric bar, which entirely fills the 0.8 cm height of the cavity, can be shifted along the straight section of the cavity. The position shown ($d=9.55$ cm) corresponds to one of the positions we used in our experiments.

depths of the coupling antennas to ensure that we missed no levels up to a certain frequency, obtaining 50 such resonant frequencies ν_j, $j=1,\ldots,50$. The corresponding wave numbers are $k_j=2\pi\nu_j/c$. We define the ''energies'' $E_j=k_j^2$. In order to extract the oscillating part of the level density $\tilde{\rho}$ from the measured data, we need the mean staircase function $\overline{\mathcal{N}}(E)$, i.e., the number of resonances up to the energy E. According to Eq. (2.22) the first two terms in a systematic expansion of $\overline{\mathcal{N}}(E)$ in powers of E are given by $\overline{\mathcal{N}}(E)=\alpha E-\beta\sqrt{E}$, where $\alpha=A/4\pi$ and $\beta=L/4\pi$. With the measured dimensions of the cavity given in Fig. 6(a) and with a conservative estimate of their uncertainties, we obtain $\alpha=22.0(5)$ cm^2 and $\beta=4.87(8)$ cm. A least-squares fit of the measured staircase of cavity resonances yields $\alpha=22.2$ cm^2 and $\beta=4.89$ cm; both agree with theoretical expectations based on measured dimensions.

For an empty billiard the classical actions in Eq. (2.15) are given by $S_n(E)=\oint_{\gamma_n}\vec{p}\cdot d\vec{x}=\hbar k l_n$, where l_n is the geometric length of the periodic orbit γ_n. Since the actions scale as $\sqrt{E}$ and the round-trip times $T_n(E)$ scale as $1/\sqrt{E}$, a Fourier transform of $\tilde{\rho}(E)$ shows peaks at the lengths l_n of periodic orbits. We determined the density of states for the empty Bunimovich stadium according to $\rho(E)=\Sigma_{j=1}^{50}\delta(E-E_j)$, subtracted the mean density $\overline{\rho}(E)=d\overline{\mathcal{N}}(E)/dE$ to obtain $\tilde{\rho}(E)$, and computed

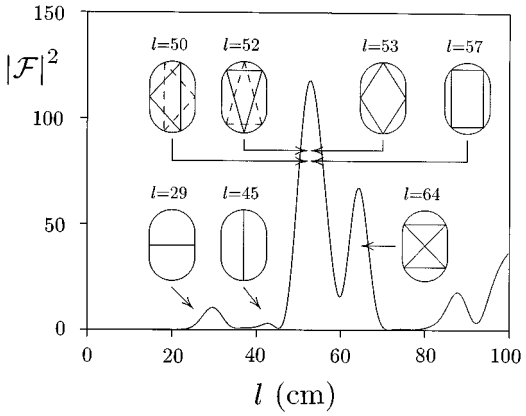

FIG. 7. Absolute square of the Fourier transform of the fluctuating part of the density of resonances of the empty cavity shown in Fig. 6(a). The assignment of peaks of $|\mathcal{F}(l)|^2$ to simple, periodic orbits is shown along with the length l of each such orbit in centimeters.

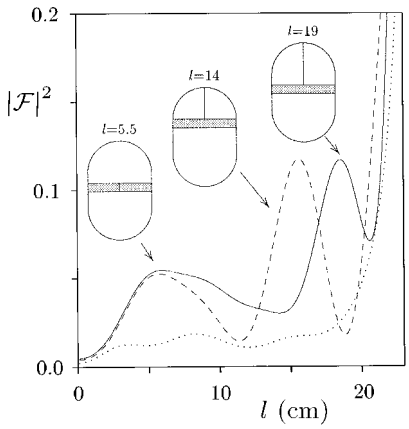

FIG. 8. Absolute square of the Fourier transform of the fluctuating part of the density of resonances shown on an expanded vertical and horizontal scale over the interval $0 \leqslant l \leqslant 23$ cm. Dotted line, empty cavity; solid line, Teflon dielectric inserted (case D_1, $d=9.55$ cm); dashed line, Teflon dielectric inserted (case D_2, $d=7.17$ cm). The assignment of peaks in the transform to simple, periodic non-Newtonian RS orbits is shown along with the optical path length l for each such orbit given in centimeters.

$$\mathcal{F}(l)=\int_0^{E_{max}}\tilde{\rho}(E)\omega(E)\exp(-ikl)dE, \qquad (3.1)$$

where $E_{max}=E_{50}$ and $\omega(E)=\sin(E/E_{max})$ is a window function that suppresses the Gibbs overshoot phenomenon [21]. Figure 7 shows the absolute square of $\mathcal{F}(l)$. As expected, we see pronounced peaks near the lengths of certain periodic orbits. As shown in Fig. 7, the large peak at $l\simeq 52$ cm covers several unresolved periodic orbits. As is discussed in Sec. VII, we estimate that thousands of levels would be needed to resolve them in this cluster. It is important to note that for the empty cavity no significant peak in $|\mathcal{F}(l)|^2$ occurs below $l=20$ cm.

IV. DIELECTRIC-LOADED CAVITY

This section demonstrates the existence of non-Newtonian orbits in the presence of ray splitting. To achieve this goal we went beyond the conventional empty billiard experiments (see Secs. I and III) by introducing a bar of Teflon dielectric into the Bunimovich cavity described in Sec. III. Experiments of this type were previously suggested in Ref. [2]. Figure 6(b) shows the shape, placement, and dimensions of the dielectric bar. In our experiments it was possible to slide the bar parallel to the major axis of the stadium using the distance d from one tip of the cavity to describe its position. Figure 6(b) shows the bar for one of the placements we used in our experiments. The dielectric constant of Teflon is known experimentally [22] to be $\epsilon=2.08$, with essentially no frequency dependence over the range of interest in this paper [23].

We studied two cases corresponding to two different placements of the dielectric bar: (D_1) $d=9.55$ cm and (D_2) $d=7.17$ cm. For each case we measured the first 50 resonance frequencies and performed the windowed Fourier transform as described in Sec. III [see Eq. (3.1)]. For the correct interpretation of our Teflon experiments it is important to realize that the Teflon bar exerts a *global* effect on the frequency spectrum: It shifts the positions of *all* resonances in the frequency domain. For the discussion below, one should not try to focus on what adding the Teflon bar might do to any individual resonance in the frequency domain; rather, one should focus on what it does to the spectrum as a whole and, in particular, to its Fourier transform. While despite the presence of the bar the appearance of the Fourier transform for $l>20$ cm is essentially unchanged, striking features appear for $l<20$ cm. On an expanded scale, Fig. 8 shows $|\mathcal{F}(l)|^2$ for the empty cavity (dotted line) and the two dielectric cases D_1 (full line) and D_2 (dashed line). While even on the expanded scale the transform for the empty stadium shows no significant structure below $l=20$ cm, the case D_1 shows two peaks, one at $l\simeq 5.5$ cm and another at $l\simeq 19$ cm. The peak at $l\simeq 5.5$ cm can be explained as the signature of a family of periodic non-Newtonian orbits bouncing inside the dielectric bar parallel to the major axis of the stadium. Inside the dielectric the action of a periodic orbit is multiplied by the index of refraction. In other words, the length of a periodic orbit is not the geometric length but the optical path length. With the dimensions given in Fig. 6 we predict that the optical path length of this orbit bouncing inside the Teflon bar is $l_{opt}=2\times\sqrt{\epsilon}\times 1.9$ cm $=5.5$ cm. This is in excellent agreement with the location of the first peak of D_1. The second peak of D_1 can be interpreted as a non-Newtonian RS orbit bouncing between the round tip of the cavity and the nearest edge of the Teflon bar [24]. Since this orbit travels entirely outside the dielectric, its optical path length should equal its geometric length, $l=2\times 9.55$ cm $=19.1$ cm. This agrees well with the experimental data. Note that shifting the location of the Teflon bar should not influence the location of the non-Newtonian ''internal bounce'' orbit at $l\simeq 5.5$ cm. Indeed, the first peak in the Fourier trans-

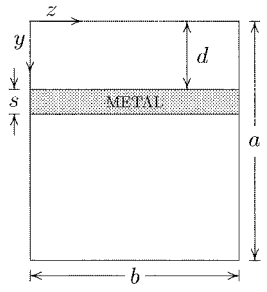

FIG. 9. Sketch of the rectangular cavity loaded with the metallic bar. In analogy to the dielectric-loaded Bunimovich stadium [see Fig. 6(b)] the metal bar can be shifted in the y direction. The position shown corresponds to one of the placements used in our experiments (M_2, $d=8.5$ cm). The dimensions of the cavity are $a=23$ cm, $b=20$ cm, and $s=2.38$ cm.

form of D_2 occurs at the same position as the peak in the D_1 data. We expect that the non-Newtonian orbit bouncing outside the dielectric, however, should shift to the new position $l=2\times 7.17$ cm $=14.34$ cm. Experimentally, the second peak in D_2 does occur near this expected position.

The reason for the non-Newtonian nature of the internal and external bounce orbits identified in our experiments is the following. As shown in Ref. [2], the Helmholtz equation for the two-dimensional cavity (partially) filled with dielectric can be interpreted as a Schrödinger equation with an attractive potential over the extension of the dielectric. Since an internal bounce orbit is one that bounces at normal incidence and at *positive* energy *inside* an everywhere negative (attractive) potential, it cannot correspond to a Newtonian orbit. The same reasoning applies to orbits bouncing off the dielectric interface at normal incidence from the outside. In the Newtonian case a trajectory normally incident on an attractive potential is transmitted with probability one. Therefore, the peaks observed near $l=19$ and 14 cm cannot originate from Newtonian periodic orbits.

This result concludes our demonstration of the signature of non-Newtonian orbits in the resonance spectrum of a particular ray-splitting system, the dielectric-loaded cavity in the shape of a Bunimovich stadium. To strengthen our claim of the universality of the presence of non-Newtonian orbits in any RS system, we now turn to an investigation of ray-splitting phenomena in thin, metal-loaded microwave cavities.

V. METAL-LOADED CAVITIES

We studied experimentally a thin rectangular cavity of dimensions $H=1.2$ cm (height), $a=23$ cm (length), and $b=20$ cm (width), with a metallic bar insert (see Fig. 9). The metallic bar is of width $b=20$ cm and has a rectangular cross section $h\times s$, where $h=0.42$ cm (height) and $s=2.38$ cm (length). In analogy to the dielectric case, we denote the distance of the bar from the nearest end wall of the cavity by d. We also find it convenient to define the coordinate system for the cavity shown in Fig. 9, associating the direction of the width of the cavity with z, the direction of the length of the cavity with y, and the direction of the height of the cavity

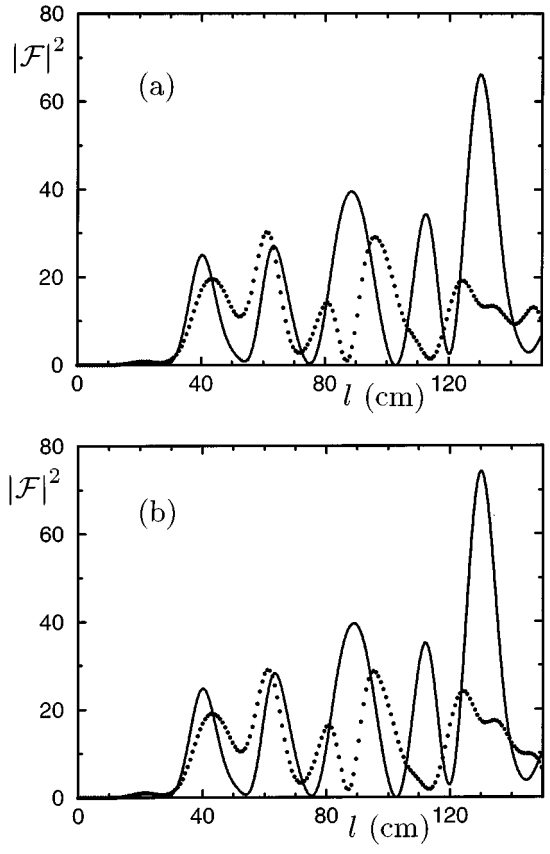

FIG. 10. Fourier transform of the level density of the 20×23 cm^2 rectangular cavity in the range $0\leqslant l\leqslant 140$ cm. Solid line, metal bar in position M_1 ($d=5$ cm); dotted line, metal bar in position M_2 ($d=8.5$ cm). (a) Experimental results. (b) Theoretical results.

with x (not shown in Fig. 9). In our experiments we investigated the spectrum of the cavity for two different positions of the metallic bar: M_1, $d=5$ cm and M_2, $d=8.5$ cm. For each position of the bar we measured the first 54 resonance frequencies and calculated the (windowed) Fourier transforms of the corresponding level densities [Fig. 10(a)]. Figure 11(a) shows the structure of the peaks associated with non-Newtonian RS orbits on an expanded scale in the range $l\leqslant 30$ cm.

Ray-splitting occurs near the sharp front and back edges of the metallic bar insert. For metallic steps no refraction occurs and the optical path length is equal to the geometric path length [2]. For the two bar positions we predict the following primitive, non-Newtonian, periodic orbits with geometric lengths $l<30$ cm that involve no more than two reflections at the edges of the metallic bar. M_1: $l=4.76$, 10, 14.76, 24.76 cm; M_2: $l=4.76$, 17, 21.76, 24.24, 29 cm. The three peaks in each of the panels of Fig. 11 (one in the dotted line, two in the solid line) account for at least three of the listed periodic orbits. As was the case for the Bunimovich stadium, see Secs. III and IV, a much larger number of eigenfrequencies would be needed to resolve all structures in the two Fourier transforms. Many of the other expected RS peaks (in particular the ones expected at $l=2s=4.76$ cm) are either too small to be seen on the scale of Fig. 11, or they are hidden in larger peaks or in steeply rising wings.

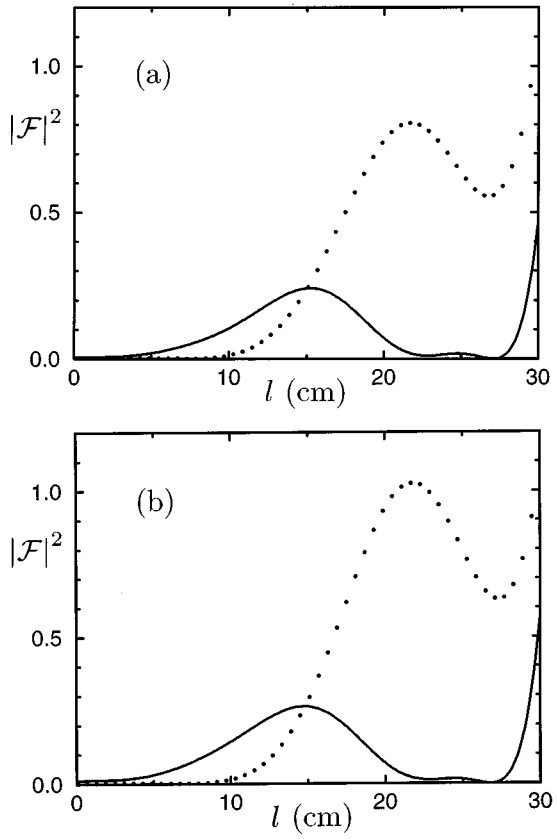

FIG. 11. Same as Fig. 10, but on a vertically and horizontally expanded scale in the range $0 \leqslant l \leqslant 30$ cm.

A rectangular cavity loaded with a metallic bar is particularly well suited for numerical calculations of its eigenmodes and eigenfrequencies. Figure 9 shows three important properties of our cavity: (i) The cross section of the cavity orthogonal to the z direction does not depend on the position, (ii) the height of the cavity is much smaller than its other two dimensions, and (iii) the cavity interior consists of three regions of simple rectangular shape. Each of these properties plays an important role in our analysis. The constancy of the cross section along the z direction allows one to treat the cavity as a section of an infinite waveguide, closed on both its ends by conducting walls. Because our cavity is thin, a large number of TE resonances occur for frequencies below the lowest-order resonance of the TM type. In this way we avoid the vector nature of the electromagnetic field. Finally, the rectangular shape of all three cavity subregions simplifies the calculations.

The starting point of the analysis is to utilize the waveguidelike shape of the cavity. This property causes the existence of the basic TE and TM field polarizations as well as guaranteeing that any solution can be expanded into propagating modes of the type $\mathbf{X}(\mathbf{r}) = \mathbf{X}(x,y)\exp(i\beta z)$. Here $\mathbf{X}$ denotes any of the electromagnetic field vectors and β is the (real) propagation constant of the mode. (We take all metal to have infinite conductivity.) The time dependence $\exp(-i\omega t)$ is implied. For the TE modes the following relationships hold:

$$\mathbf{E}_\perp = i\frac{\mu_0\omega}{\beta^2-k^2}\mathbf{e}_z\times\nabla_\perp H_z(\mathbf{r}), \tag{5.1}$$

$$\mathbf{H}_\perp = -i\frac{\beta}{\beta^2-k^2}\nabla_\perp H_z(\mathbf{r}). \tag{5.2}$$

It follows that all field components can be obtained from $H_z(\mathbf{r})$ alone. Note that for TE polarization $E_z = 0$, so the electric field vector remains in the xy plane.

For $\mathbf{E}$ and $\mathbf{H}$ to fulfill Maxwell's equations, H_z must satisfy the two-dimensional Helmholtz equation everywhere inside the cavity

$$\nabla_\perp^2 H_z(x,y) + \kappa^2 H_z(x,y) = 0, \tag{5.3}$$

with the boundary conditions

$$\mathbf{n}\cdot\nabla_\perp H_z = 0. \tag{5.4}$$

The symbols used above have the usual meaning: the subscript $\perp$ denotes the transverse part of a vector or an operator, ∇ is the gradient operator, $\mathbf{e}_z$ is the unit vector in the z direction, $\mathbf{n}$ is the unit vector perpendicular to the cavity boundary, $k = \omega/c$ is the wave number, c is the velocity of light, and μ_0 is the permeability of vacuum. The parameter κ in the Helmholtz equation (5.3) is the transverse wave number, which is related to the propagation constant β and the wave number k by

$$k^2 = \beta^2 + \kappa^2. \tag{5.5}$$

At the walls $z = 0$ and $z = b$ of the cavity the transverse component of the electric field must vanish. In order to match these conditions the allowed values of the parameter β are $\beta_n = n(2\pi/c)$, $n = 1,2,\ldots$.

This establishes the longitudinal dependence of the field. It is of the form $\sin(\beta_n z)$ for E_x, E_y, and H_z and of the form $\cos(\beta_n z)$ for H_x and H_y. The occurrence of sine and cosine form factors is related to the different symmetry properties of the various field components under the transformation $\beta \rightarrow -\beta$. But what about the transverse characteristics? To answer this question we have to solve Eq. (5.3) together with Eq. (5.4). This yields the allowed values κ_m for the transverse wave number κ and, of course, the transverse field $H_z(x,y)$. The (dispersion) relation

$$\omega_{mn} = c\sqrt{\kappa_m^2 + \beta_n^2} \tag{5.6}$$

gives the resonant frequencies. The central question now is how to find the κ_m's. We begin by making use of the simple shape of the cavity. Because the cross section can be split into three rectangular sections: (I) $0<x<H$, $0<y<d$; (II) $h<x<H$, $d<y<d+s$; and (III) $0<x<H$, $d+s<y<a$, $H_z(x,y)$ can be expanded in a Fourier series of the form

$$H_z(x,y)=\begin{cases}\displaystyle\sum_{n=0}^{\infty} A_n\cos(\eta_n y)\cos(\gamma_n x) & \text{(I)}\\ \displaystyle\sum_{n=0}^{\infty}\{C_n\cos[\zeta_n(y-\overline{a})]+D_n\sin[\zeta_n(y-\overline{a})]\}\cos[\delta_n(x-h)] & \text{(II)}\\ \displaystyle\sum_{n=0}^{\infty} B_n\cos[\eta_n(a-y)]\cos(\gamma_n x) & \text{(III)}.\end{cases} \tag{5.7}$$

The new symbols are $\overline{a}=d+s/2$ (the position of the center of the bar), $\gamma_n=n\pi/H$, $\delta_m=m\pi/(H-h)$, $\eta_n=\sqrt{\kappa^2-\gamma_n^2}$, and $\zeta_n=\sqrt{\kappa^2-\delta_n^2}$. The coefficients A_n, B_n, C_n, D_n are the Fourier amplitudes to be determined. It is possible to prove that Eq. (5.7) solves the Helmholtz equation (5.3) and matches the required boundary condition (5.4) at all cavity walls. What remains is to ensure the continuity of the field that crosses the subregions boundaries at $y=d$ and $y=d+s$ and to match the boundary conditions (5.4) at both faces of the metallic bar.

The remaining steps are straightforward. One chooses large enough numbers N_{max} and M_{max} of the Fourier components in the corresponding subregions I and III, and II, respectively, and sufficiently large numbers of mesh points at the boundaries $y=d$ and $y=d+s$. Then, by imposing the continuity and boundary conditions at each mesh point one obtains a set of linear equations for the amplitudes A_n, B_n, C_n, D_n. A correct choice of numbers makes the number of equations equal the number of unknown amplitudes. Therefore, a nontrivial solution exists if the determinant of the corresponding matrix of coefficients $\mathbf{M}$ is zero. Since the matrix elements still depend on the parameter κ, the equation

$$\text{Det } \mathbf{M}(\kappa)=0 \tag{5.8}$$

is the desired equation for the κ_m's and thus determines the resonance frequencies of the cavity. The last two steps, i.e., the computation of the determinant and the calculation of the zeros of Eq. (5.8), were done numerically.

We used the theoretical method described above to make calculations for several rectangular cavities with the metallic bar placed in the positions M_1 and M_2. First we compared calculated eigenfrequencies with measured ones and found good agreement. Over the range 2–6 GHz discrepancies were on the order of several megahertz, which we attribute to small imperfections of the shape of the experimental cavity. The Fourier transforms of the theoretically calculated level density for the experimental cavity with the metallic bar in positions M_1 and M_2 are shown in Figs. 10(b) and 11(b); they show excellent agreement with the respective Fourier transforms of the experimental resonance data.

In order to get a closer look at the non-Newtonian RS orbits we calculated the first 972 resonances (frequency range 0–12.5 GHz) of a larger rectangular cavity with the following dimensions: $b=40$ cm, $a=46$ cm, and $H=1.2$ cm. The metallic bar insert had the same rectangular cross section as was used in the experiment and it was placed in positions M_1 and M_2, respectively. Figure 12 shows the Fourier transforms of the level density for $0\leqslant l\leqslant 50$ cm. The shape of the peaks and the shoulders in the Fourier transform suggests that for the bar in position M_1 the non-Newtonian RS orbits have the length $l\simeq 10$ and 14.8 cm and for the bar in position M_2 $l\simeq 17$ and 21.8 cm, respectively. This agrees with our expectations. The internal bounce periodic orbit peak expected near $l=4.76$ cm in the M_1 transform is obscured by the steeply rising wing at $l\approx 5$ cm, but it is barely visible as a small peak in the M_2 transform. The length of the M_2 analog of the M_1 periodic orbit that occurs at $l=24.76$ cm is $l=38.76$ cm. It is responsible for the dotted peak at $l\approx 40$ cm in Fig. 12.

We did another set of calculations for a rectangular cavity of the following dimensions: $b=80$ cm, $a=92$ cm, and $H=1.2$ cm. The metallic bar had a 4.2 mm height and a 10 cm width. It was placed in position M_1. We calculated 3959 resonances from 0 to 12.5 GHz. Presented in Fig. 13, the Fourier transform of the calculated level density shows peaks (shoulders) very close to the expected positions for non-Newtonian RS orbits, which are predicted to occur at $l=10$, 20, 30, and 40 cm, respectively.

VI. SEMICLASSICAL ANALYSIS

Locations, widths, and heights of the non-Newtonian peaks shown in Fig. 8 can be estimated semiclassically. In order to illustrate the procedure, we focus on the non-Newtonian external bounce orbit, which, for case D_2, occurs at $l\approx 14$ cm. On the basis of the theoretical framework provided in Refs. [2,4], we obtain its contribution to the oscillating part of the scaled density of resonances as

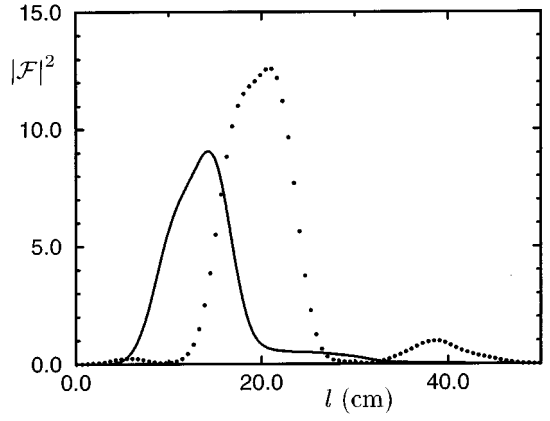

FIG. 12. Theoretical computation of the Fourier transform of the level density of the rectangular metal-loaded 40×46 cm^2 cavity in the range $0\leqslant l\leqslant 50$ cm. Solid line, case M_1, dotted line, case M_2.

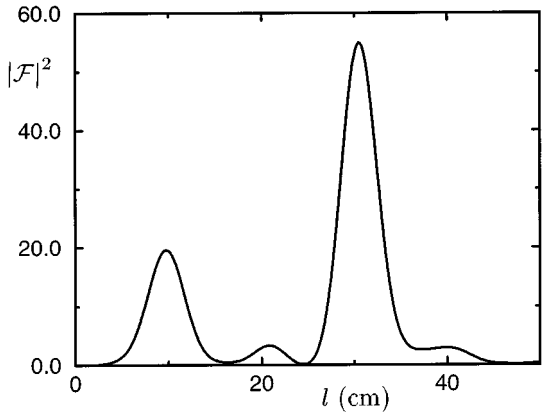

FIG. 13. Theoretical computation of the Fourier transform of a large rectangular metal-loaded cavity. Size of the cavity, 80×92 cm^2; width of the metal bar, 10 cm; position of the bar, M_1 ($d=5$ cm).

$$\tilde{\rho}_s(E)=(Rr/2\pi k)\sin(2kR), \tag{6.1}$$

where

$$r=\frac{1-\sqrt{\epsilon}}{1+\sqrt{\epsilon}} \tag{6.2}$$

is the reflection coefficient and $R=7.17$ cm is the radius of the circular end cap of the cavity (see Fig. 6). The Fourier transform (3.1) of $\tilde{\rho}_s(E)$ can be performed analytically for $\omega=1$. Neglecting an additive nonresonant term, we obtain

$$|\mathcal{F}(l)|^2=\frac{R^2r^2}{4\pi^2}\,\frac{\sin^2[(2R-l)K/2]}{[(2R-l)/2]^2}, \tag{6.3}$$

where $K=\sqrt{E_{50}}\approx1.54$ cm^{-1}. For large K Eq. (6.3) becomes

$$|\mathcal{F}(l)|^2\rightarrow\frac{R^2r^2}{2\pi}K\delta(2R-l). \tag{6.4}$$

This result shows that in the limit of large K isolated non-Newtonian orbits indeed contribute a δ-function singularity to $\mathcal{F}(l)$, as was conjectured in Sec. II on the basis of Eq. (2.15). In addition, Eq. (6.4) confirms that the location of the external bounce orbit is indeed expected at $l=2R\approx14$ cm. For finite K we obtain peaks broadened in l with full width at half maximum (FWHM) of

$$\Gamma\approx5.57/K. \tag{6.5}$$

In the present case $\Gamma\approx3.6$ cm, which agrees well with the widths of the peaks at $l\approx14$ and 19 cm in Fig. 8. We define the strength of a peak to be $\sigma=\int|\mathcal{F}(l)|^2dl$. According to Eq. (6.4), we expect $\sigma=0.41$ cm. Estimating the strength of the peak at $l\approx14$ cm in Fig. 8 as its height times its FWHM, we obtain $\sigma\approx0.43$ cm. The experimental result and the theoretical estimate for the strength are close. Though encouraging, this agreement is fortuitous for the following reasons. (i) The Fourier transform of the experimental resonances contains a window function. If it is taken into account, it reduces the theoretical estimate of the strength by a factor 4. (ii) Over the whole range of the 50 resonances used in the Fourier transform, the level density $\tilde{\rho}_s(E)$ exhibits only about three oscillations. We expect that the full information on the non-Newtonian orbit is not yet contained in such a small number of oscillations. Consequently, the heights of the peaks in Fig. 8 are not yet converged in the number of resonances. We confirmed this by computing $|\mathcal{F}(l)|^2$ with inclusion of 40, 45, and 50 resonances in the transform (3.1).

VII. DISCUSSION

There are several points about our experiment and its theoretical interpretation that need to be discussed. Let us start with the number of states used in our experiments with the dielectric bar. The present evaluation of our data is based on only the first 50 states. This does not mean that we were unable to measure more resonances, but it does mean that above $\mathcal{N}\approx50$ we could not guarantee that we would not miss any levels. With the help of theoretical calculations we found that missing a level has disastrous consequences for locations, heights, and even the very appearance of the non-Newtonian peaks in the Fourier transform. This explains why, from the experimental point of view, we had to restrict ourselves to a ''safe'' range of resonances, here 50.

With 50 states we are able to resolve the non-Newtonian peaks in the experiments with the dielectric bar, but we are unable to resolve the cluster of Newtonian peaks in Fig. 7. The smallest distance between peaks in this cluster is $\Delta l\approx1$ cm. To resolve the associated peaks one should aim at a resolution of $\Gamma<0.2$ cm, where Γ is the width of the associated Newtonian peaks. Assuming that the shape of these peaks is essentially given by Eq. (6.3), we use Eq. (6.5) to estimate the minimum necessary wave number K_{min} for the required resolution. We obtain $K_{min}=5.57/0.2$ cm ≈28 cm^{-1}. According to the leading term of the mean staircase function $\overline{\mathcal{N}}(E)$ derived in Sec. III, this means that the Fourier transform should be based on at least $\mathcal{N}\approx\alpha K_{min}^2\approx18\,000$ states. This is obviously way beyond the reach of our present experiment and it is also beyond the number of resonances ($\sim10^3$) being investigated in recent experiments with empty, superconducting cavities; see, e.g., Ref. [25]. Therefore, given the present state of the experimental art, we did not even attempt a microwave cavity experiment that would be able to fully resolve thousands of resonances. However, our present results establish the need for improving the experimental state of the art so that converged locations and heights of RS peaks can be compared with theory.

In this connection we may point out that the discussion presented in Sec. VI presents a direct comparison of semiclassically computed peak heights, widths, and locations corresponding to non-Newtonian RS orbits with peaks resulting either from a numerical solution of the Schrödinger equation or from direct experimental measurements. Another important point presented is the extraction of information on non-Newtonian orbits from our computations of the resonances of the metal-loaded cavity reported in Sec. V. In our computations we take the vector nature of the electromagnetic field explicitly into account. This is important since a metallic step, which does not fill the full height of a two-dimensional cavity, generates a fringe field that is inhomogeneous over the height of the cavity. Thus the magnitude of the electric field in the vicinity of a metallic step depends nontrivially on

all three spatial dimensions. Qualitatively, the same considerations apply if an inserted dielectric bar does not fill the entire height of the cavity. Thus the one-to-one correspondence with the Schrödinger equation can be broken locally near the step. Therefore, in metal-loaded cavities a reasonably sharp RS boundary (and thus nearly global equivalence with a Schrödinger equation) occurs only if the wavelength is much larger than the spatial extent of the inhomogeneity of the electromagnetic field in the step region. Metal-bar-loaded cavities are very similar to ''two-height'' cavities whose investigation in the context of ray splitting was suggested earlier in Ref. [2].

As part of a more general discussion of our experiment, let us emphasize what is different about non-Newtonian RS orbits in the Fourier domain as opposed to resonances in the frequency domain. The central point of our work is not the emergence of individual, different frequency resonances connected with waves bouncing inside and outside the dielectric, resonances whose frequencies can be computed from the optical path length of the non-Newtonian orbits identified in our experiments. If this were the central point of our paper, nothing would be different about our experiment since resonances of this nature are routinely used in (Fabry-Pérot or other) interferometers in many laboratories around the world. But this is not so. The non-Newtonian orbits we find experimentally are associated with peaks that appear in the *Fourier transform* of the *total set of all cavity resonances* only when the dielectric bar or metal step is put into the cavity. Once this difference is appreciated, the peaks in the Fourier transform are both different and surprising.

In this paper it is not our intention to dwell on the deeper nature of the non-Newtonian orbits identified in our experiments. Rather, our present goal is to prove the existence of non-Newtonian orbits by using their characteristics as far as they are established in the literature. We are not aware of any published papers that predict more about the non-Newtonian orbits than we established experimentally. We hope, however, that our paper will inspire further theoretical work on the nature of the non-Newtonian orbits now that we have proved their existence experimentally beyond any reasonable doubt.

In particular we think that prebifurcation ghosts [26] have nothing to do with the non-Newtonian RS orbits that we find in our experiments. For instance, it is known [26] that prebifurcation ghosts disappear exponentially as a function of energy. On the other hand, it is easily seen by a high-energy expansion of Eq. (2.20) that the reflection coefficient vanishes only as a power law in the energy. Thus, contrary to the behavior of prebifurcation ghosts, our non-Newtonian orbits continue to be important at high energies. We think that this behavior establishes a profound difference between our non-Newtonian orbits and the ghost orbits discussed in the literature. Moreover, our non-Newtonian orbits are not the result of complex solutions in a complexified phase space. Rather they occur as a result of a boundary condition imposed at the ray-splitting surface. However, we should point out that inclusion of the ghost contributions in Eq. (2.15) would certainly improve the agreement between the semiclassical theory of RS systems and the complete quantum-mechanical theory. As a matter of fact, since non-Newtonian periodic orbits undergo much the same type of bifurcations as Newtonian periodic orbits, we expect contributions to Eq. (2.15) from Newtonian as well as non-Newtonian ghosts. Identifying and evaluating these non-Newtonian ghost contributions quantitatively must be left for future work.

VIII. SUMMARY AND CONCLUSIONS

The main thrust of our paper is to present experimental and theoretical evidence for the existence of non-Newtonian orbits produced by ray splitting in dielectric- and metal-loaded cavities that are of relevance to the context of quantum chaos. All our experimental results are corroborated and supported by detailed numerical calculations and interpreted within the framework of the extended Gutzwiller formula (2.15). For the location and height of a particular type of non-Newtonian orbit we obtained qualitative agreement with the results of semiclassical calculations.

Based on the discussion presented in Sec. VII, we conclude that our experiments and accompanying theory establish beyond any reasonable doubt the existence, widths, and locations of peaks in the Fourier transform of $\tilde{\rho}(E)$ that can be associated with non-Newtonian periodic orbits. Since ray splitting occurs in all wave systems with sharp, partially transparent interfaces we expect the signatures of non-Newtonian RS orbits in $\tilde{\rho}(E)$ as a universal feature of all RS wave systems.

ACKNOWLEDGMENTS

We gratefully acknowledge fruitful discussions on ghost orbits and non-Newtonian orbits with Professor F. Haake and Dr. L. Westling. L.S. acknowledges the hospitality of the Physics Department during his stay at Stony Brook. Sz.B., A.B., and L.S. acknowledge partial support by KBN Grant No. 2 P03B 093 09 and P.M.K. acknowledges financial support from NSF Grant No. PHY94-23001. R.B. gratefully acknowledges financial support by the Deutsche Forschungsgemeinschaft.

[1] L. Couchman, E. Ott, and T. M. Antonsen, Jr., Phys. Rev. A **46**, 6193 (1992).
[2] R. E. Prange, E. Ott, T. M. Antonsen, Jr., B. Georgeot, and R. Blümel, Phys. Rev. E **53**, 207 (1996).
[3] M. C. Gutzwiller, *Chaos in Classical and Quantum Mechanics* (Springer, New York, 1990).
[4] R. Blümel, T. M. Antonsen, B. Georgeot, E. Ott, and R. E. Prange, Phys. Rev. Lett. **76**, 2476 (1996); Phys. Rev. E **53**, 3284 (1996).
[5] R. Blümel and A. Kohler, Phys. Bl. **52**, 1243 (1996).
[6] L. Sirko, P. M. Koch, and R. Blümel, Phys. Rev. Lett. **78**, 2940 (1997).
[7] G. Vattay, A. Wirzba, and P. E. Rosenqvist, Phys. Rev. Lett. **73**, 2304 (1994).

[8] H.-J. Stöckmann and J. Stein, Phys. Rev. Lett. **64**, 2215 (1990).
[9] S. Sridhar and A. Kudrolli, Phys. Rev. Lett. **72**, 2175 (1994).
[10] L. C. Maier, Jr., and J. C. Slater, J. Appl. Phys. **23**, 68 (1954).
[11] S. Sridhar, Phys. Rev. Lett. **67**, 785 (1991).
[12] P. So, S. M. Anlage, E. Ott, and R. N. Oerter, Phys. Rev. Lett. **74**, 2662 (1995).
[13] U. Stoffregen, J. Stein, H.-J. Stöckmann, M. Kuś, and F. Haake, Phys. Rev. Lett. **74**, 2666 (1995).
[14] W. H. Miller, Adv. Chem. Phys. **25**, 69 (1974).
[15] L. D. Landau and E. M. Lifshitz, *Quantum Mechanics*, 3rd ed. (Pergamon, Oxford, 1977); see Sec. 25, problem 3.
[16] R. N. Oerter, E. Ott, T. M. Antonsen, Jr., and P. So, Phys. Lett. A **216**, 59 (1996).
[17] A. Kohler, G. H. M. Killesreiter, and R. Blümel, Phys. Rev. E **56**, 2691 (1997).
[18] J. D. Jackson, *Classical Electrodynamics* (Wiley, New York, 1975).
[19] A. Kudrolli, S. Sridhar, A. Pandey, and R. Ramaswamy, Phys. Rev. E **49**, R11 (1994).
[20] S. Deus, P. M. Koch, and L. Sirko, Phys. Rev. E **52**, 1146 (1995).
[21] See J. S. Walker, *Fast Fourier Transforms* (CRC, Boca Raton, FL, 1991). We checked that all non-Newtonian orbits discussed in this paper were insensitive to the choice of window function $\omega(E)$. We reproduced essentially the same locations and relative heights of the peaks shown in Figs. 7 and 8 with $\omega(E)=\sin(\sqrt{E/E_{max}})$, $\sin^2(\sqrt{E/E_{max}})$, and $\sin^2(E/E_{max})$.
[22] K. H. Breeden and A. P. Sheppard, Microw. J. **10**, 59 (1967); Radio Sci. **3**, 205 (1968).
[23] The loss of Teflon is so low (loss tangent $\lesssim 0.0004$; see Ref. [22]) that we found that introducing the Teflon bar into the present cavity did not lower the average $Q=\nu/\Delta\nu$ of the observed resonances. In fact, we found that the average Q rose slightly because the Teflon increased the effective volume of the cavity.
[24] There will also be other peaks, e.g., caused by a non-Newtonian RS orbit bouncing between the round tip of the cavity and the farthest edge of the Teflon bar. Its length for case (D_1) $[(D_2)]$ would be 24.6 cm [19.8 cm], causing it to be ''lost'' in the giant peak rising near $l=20$ cm in Fig. 8. The peaks discussed in the text associated with the shortest non-Newtonian RS orbits are the only ones easily resolved in the present geometry.
[25] H. Alt, H.-D. Gräf, H.L. Harner, R. Hofferbert, H. Lengeler, A. Richter, P. Schardt, and H. A. Weidenmüller, Phys. Rev. Lett. **74**, 62 (1995).
[26] M. Kuś, F. Haake, and D. Delande, Phys. Rev. Lett. **71**, 2167 (1993).